FINAL TECHNICAL REPORT

Refining Earthquake Recurrence and Slip Over the Past 4 - 5 events on the Southern Santa Cruz Mountains Segment of the San Andreas Fault

Recipient:

University of Oregon
Department of Geological Sciences
1272 University of Oregon Eugene, OR 97403-1272
tel (541) 346-4584; fax (541) 346-4692; URL http://pages.uoregon.edu/dogsci/doku.php

Principal Investigators:

Ashley R. Streig[1], Ray J. Weldon II [2], Timothy E. Dawson[3]
streig@uoregon.edu[1], ray@uoregon.edu[2], Timothy.Dawson@conservation.ca.gov[3]

Keywords:

San Andreas fault, Santa Cruz Mountains, earthquake chronology and recurrence

Program Element III

U. S. Geological Survey
National Earthquake Hazards Reduction Program
Award Number G12AP20094

October 2013

Research supported by the U.S. Geological Survey (USGS), Department of the Interior, under USGS award number G11AP20123. The views and conclusions contained in this document are those of the authors and should not be interpreted as necessarily representing the official policies, either expressed or implied, of the U.S. Government.

Award G12AP20094

Refining Earthquake Recurrence and Slip Over the Past 4 - 5 events on the Southern Santa Cruz Mountains Segment of the San Andreas Fault

Ashley R. Streig[1], Ray J. Weldon[1]
and Timothy E. Dawson[2]
[1]University of Oregon, [2]California Geological Survey
ray@uoregon.edu, streig@uoregon.edu, Timothy.Dawson@conservation.ca.gov

ABSTRACT

The Hazel Dell site provides the first definitive paleoseismic evidence of two pre-1906 19th century events on the Santa Cruz Mountains section of the San Andreas fault based on the presence of anthropogenic artifacts. Hundreds of pieces of cut redwood chips were found embedded in a buried soil that coincides with the ante-penultimate (E3) earthquake surface. This suggests that redwood trees at the site were cut down just before earthquake E3. We correlate our paleoseismic findings with the historic record and the onset of redwood logging in the area by determining the age of the woodchips. We wiggle match radiocarbon dates from inner and outer growth rings from two wood chips (with bark) and the known interval between growth rings, with the intercepts of the INTCAL04 terrestrial ^{14}C calibration curve. Using this technique, the youngest woodchip ring is dated to 1813 A.D. We also sampled 14 annual growth rings from a 274 ring sequence transect from a buried redwood tree stump for ^{14}C dating to further constrain the felling date of redwoods at the site. Pending ^{13}C measurements, we find that the youngest ring we have identified in the tree is A.D. 1800. There are no known ethnographic or historical accounts of pre-contact native people chopping down large trees in the way that European colonists would have. The first record of European land use was for pasture in 1803, and the property became a Spanish land grant in 1827, soon after which a whip-saw lumber mill is documented to have begun operation in the upper Corralitos area. We combine these paleoseismic results with historical earthquake accounts for the area and conclude that the San Andreas fault ruptured in 1838, 1890 and 1906.

TABLE OF CONTENTS

Abstract i
1.0 Introduction 1
2.0 Hazel Dell Road Paleoseismic Investigation Site 3
2.1 Site Geology 3
2.2 Description of Stratigraphic Units: 5
2.3 Event Chronology at the Hazel Dell site 7
2.4 Methods 8
3.0 Results 10
3.1 Radiocarbon Analysis 10
3.2 Earthquake Age Estimates 16
3.3 Improving Age Estimates: Wiggle-matching a redwood tree stump 17
4.0 Significance of results 19
5.0 Acknowledgements 19
6.0 References 20
7.0 Publications and Conference proceedings 21

LIST OF TABLES

Table 1. Radiocarbon Ages for wood chips, redwood cones & needles, and detrital charcoal from the Hazel Dell Site. 10

Table 2. Preliminary Radiocarbon Ages for annual growth rings collected from a redwood stump at the Hazel Dell Site 10

LIST OF FIGURES

Figure 1. Location map showing the Santa Cruz Mountains section of the San Andreas fault 2
Figure 2. LiDAR strip map of the Hazel Dell Road area (central SAS) 3
Figure 3. Hazel Dell site map 4
Figure 4. Stratigraphic columns and descriptions of deposits 5
Figure 5. Historical artifacts – Photos of axe-cut wood chips 8
Figure 6. Macro fossils collected from block samples 9
Figure 7. Plot of woodchip HD-2011-WC1 ^{14}C dates with the IntCal ^{14}C calibration curve and OxCal modeled date for the outermost growth ring..... 13
Figure 8. Plot of woodchip HD-2011-WC2 ^{14}C dates with the IntCal ^{14}C calibration curve and OxCal modeled date for the outermost growth ring..... 13
Figure 9. Plot of macrofossil ^{14}C dates with the IntCal ^{14}C calibration curve..... 14
Figure 10. OxCal model for Hazel Dell, modeled stratigraphic and event age estimates 15
Figure 11. Photographs and cross section of buried redwood tree stump 16

1.0 INTRODUCTION

This report presents age dating results for key stratigraphic units at the Hazel Dell Road paleoseismic investigation site on the Santa Cruz Mountains section of the San Andreas fault, located near the town of Corralitos, Santa Cruz County, California (Figure 1; 37°00'01"N, 121°44'30"W). The objective of this project was to refine stratigraphic age models and paleoearthquake timing and recurrence data at the Hazel Dell (HD) site. Improved age control for the Hazel Dell site will allow us to make direct comparisons of paleoearthquakes between sites, and build a composite earthquake chronology for the Santa Cruz Mountains section of the fault. HD is located between the Grizzly Flat paleoseismic site of Schwartz and others (1998) and the Mill Canyon and Arano Flats paleoseismic sites of Fumal (2012; 2003) (Figure1).

This project is a continuation of work in FY2008, FY2010, FY2011 at the Hazel Dell site. This grant funded additional work at the Hazel Dell site to refine age estimates for the most recent three earthquakes at the site. We collected detrital charcoal, wood chips, and block samples of key stratigraphic units for macrofossil analysis in the lab, and used all three sample types to constrain the ages of the deposits using ^{14}C dating. We returned in 2012 to re-excavate trenches from 2008 to relocate buried redwood tree stumps identified in FY2008. During the 2012 field season, we exposed shallowly buried redwood stumps at the intersection of trenches T1-T2, and T1-T6 that were 1.75 m wide and were chopped off and burned along the cut face. These stumps were rooted in unit 400, a buried soil and ground surface during the ante-penultimate earthquake, E3. We are in the process of dating a sequence of annual growth rings from one of these stumps using AMS ^{14}C techniques the preliminary results for this effort are reported herein. For additional background information and findings from earlier studies please refer to the Final Technical Report submitted to the U. S. Geological Survey National Earthquake Hazards Reduction Program for Award Numbers G10AP00065 and G10AP00064, that can be downloaded at:
http://earthquake.usgs.gov/research/external/reports/G10AP00064.pdf (Streig *et al.*, 2012 *AGU fall meeting abstracts*; Streig *et al., in press BSSA*)

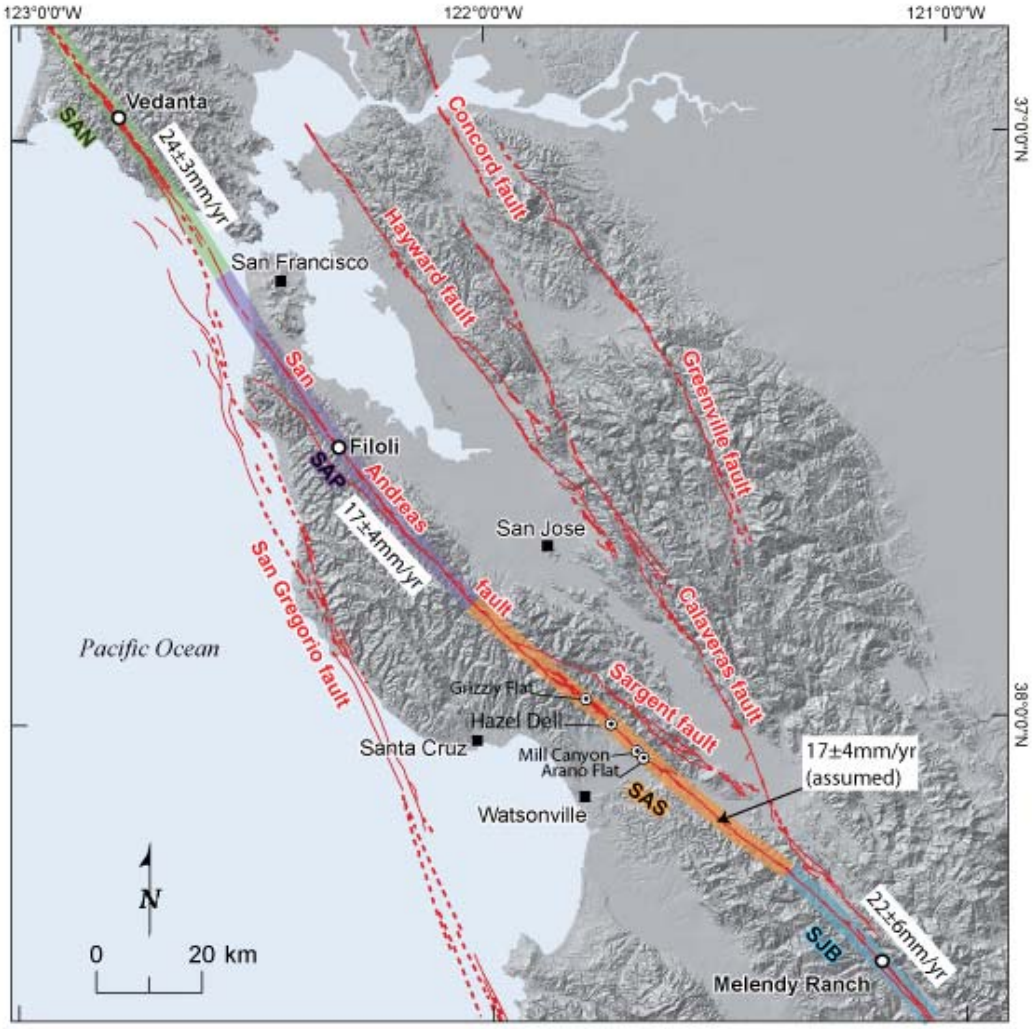

Figure 1. Location map showing the Santa Cruz Mountains section (SAS) relative to San Andreas Fault sections to the north and south (North Coast section (SAN), Peninsula Section (SAP) and the Creeping Section (SJB)) and other principal Bay Area faults. Paleoseismic investigation sites along the SAS are shown as closed circles and include (from N-S) Grizzly Flat, Hazel Dell - Simas Lake, Mill Canyon and Arano Flat sites. Geologic slip rate sites are shown as open circles and include: Vedanta on the North Coast section, Filoli on the Peninsula section and Melendy Ranch on the creeping section. Slip rates were determined at Vedanta, Filoli and Melendy sites and adopted by WGCEP 02 and 07 are shown in white boxes.

2.0 HAZEL DELL ROAD PALEOSEISMIC INVESTIGATION SITE

2.1 Site Geology

The SAF in the Hazel Dell area trends northwesterly, N30°W to N40°W (Figure 2), and bounds the western edge of the valley. Locally, the fault juxtaposes sandstone and shale of the Purisma Formation on the west against shale of the Mt. Pajaro Formation on the east (Brabb, 1989). Previous workers mapped the SAF as several complex splays; the main trace is characterized by a linear valley, aligned topographic lineaments, offset drainages, linear drainages and sag ponds (Sarna-Wojcicki and others, 1975). The currently active fault trace is located along the western edge of Hazel Dell Valley, has a relatively continuous surface trace marked by well defined linear base of slope along east-facing hillslopes bounding the valley, and aligned linear drainages and topographic escarpments south of Old Mt. Madonna Road and north of Green Valley Road respectively (Figure 2).

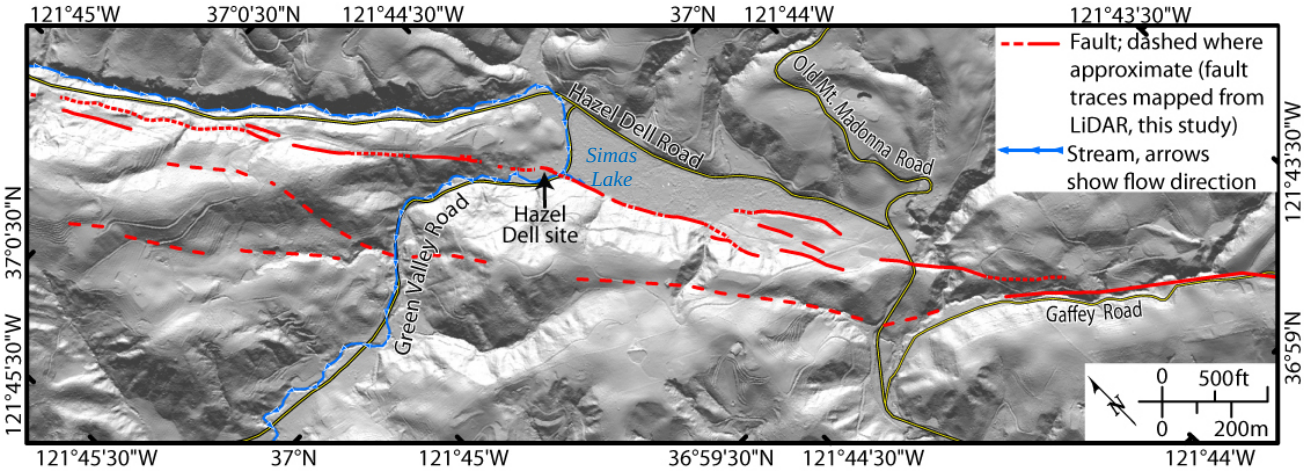

Figure 2. Detailed fault map of geomorphic lineaments in the Hazel Dell area (central SAS) generated from LiDAR data (OpenTopography/ GeoEarthScope 0.5 m data). Locally, the fault is expressed as a series of aligned drainages, linear range fronts , aligned topographic escarpments and a sharp base of slope along east-facing hillslopes. The Hazel Dell investigation site is located in the northwest corner of the fault bound valley, associated with a transtensive (right) step in the fault zone. Fault traces were mapped on 0.5 m resolution LiDAR derivatives in an earlier study (Streig *et al.*, 2012; Streig *et al., in press*). Basemap: shaded relief compiled from GeoEarthScope LiDAR data (Prentice *et al*., 2009).

The Hazel Dell trench site is located within an area of overbank deposits on the north side of Green Valley Road, is flanked by Green Valley Creek to the south and west, hillslopes of the sandstone member of the Mt. Pajaro Formation bound the site to the north and east. The creek crosses the fault at the southwest corner of the site (Figure 2). The Hazel Dell site is within the floodplain and has been inundated by flood waters in recent high rainfall years (personal communication, property owner, D. Dent, 2008). In these flood events the site was blanketed by fine-grained alluvial overbank deposits. The investigation site was an apple orchard between roughly 1950 and 1980 (personal communication property owner, D. Dent, 2008). The ground surface has been tilled, disturbing 20 to 50 cm below the ground surface in trench exposures. These farming activities combined with historic

overbank deposits obscure the surface expression of 1906 surface rupture across the site. However, 1906 offsets the youngest alluvial units across the site and evidence of the 1906 rupture is preserved in the stratigraphy and exposed in trenches.

We excavated a combination of slot and benched trenches across the site during summer and fall of 2008, 2010 and 2011 (Figure 3). Trench exposures were cleaned, gridded with a 1 m x 0.5 m string and nail grid, and photographed. All trench exposures were logged on a photo mosaic of high-resolution digital photographs at a scale of roughly 1:10. Stratigraphic units and structural relations were documented and described on photo logs (Streig *et al.*, 2012; Streig *et al., in press*). Both walls were documented in trenches that crossed the fault and fault parallel trenches adjacent to the fault. Only the north wall was documented in trenches 1, 2 and 6 that did not cross a fault trace and were located to span the site to explore for other possible fault traces. We collected detrital charcoal, wood chips, and block samples of key stratigraphic units for macrofossil analysis in the lab, and used all three sample types to constrain the ages of the deposits using ^{14}C dating. During the 2012 field season, we exposed shallowly buried redwood stumps at the intersection of trenches T1-T2, and T1-T6, that were 1.75 m wide and were chopped off. We surveyed trench outlines, faults, string grids and key stratigraphic units using a total station, and used a network of base stations and a differential GPS unit to tie together each survey and incorporate these data in an ArcGIS database (Figure 3).

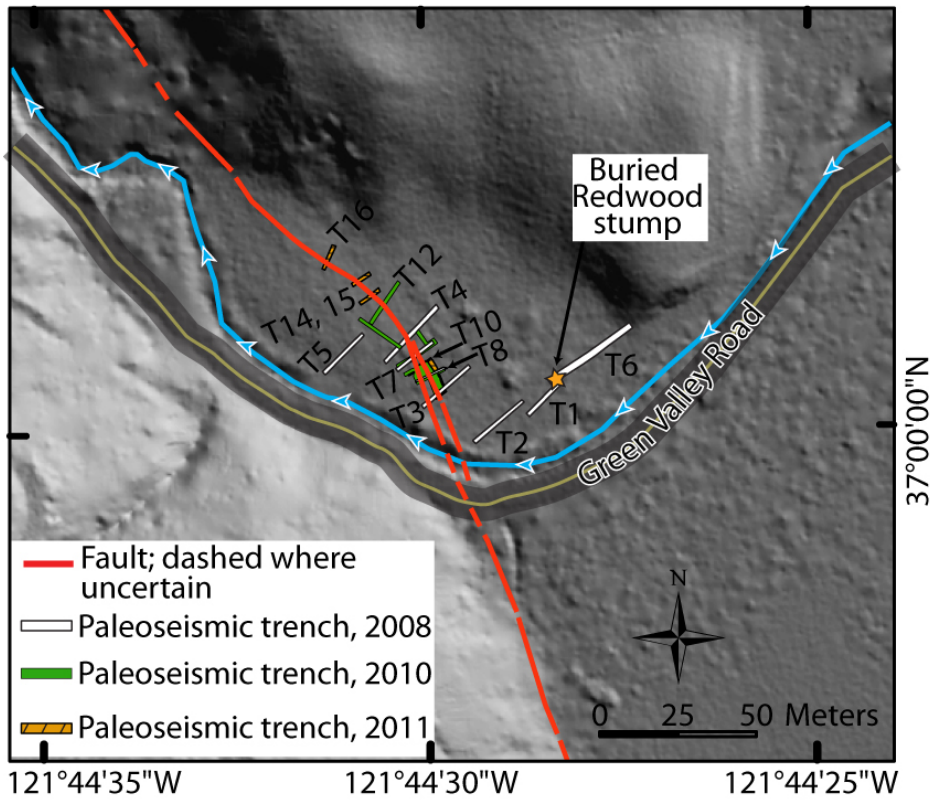

Figure 3. Hazel Dell site map showing the fault trace across the investigation site in red and the locations of 2008, 2010 and 2011 trenches, and the location of the sampled redwood tree stump. Green Valley Creek is shown in blue; arrows show flow direction. The location of a ~ 1.75 m wide redwood stump excavated summer of 2012 is shown by the orange star.

2.2 Description of Stratigraphic Units:

Trenches across the site exposed alluvial deposits sourced from Green Valley Creek, organic marsh deposits, and colluvium (Figure 4) that originated from the bedrock escarpment to the north and east. Coarse-grained alluvial deposits, medium to fine-grained alluvial stream deposits and a fine-grained alluvial marsh sequence are deposited against, and interfinger with, slope-derived colluvium proximal to hillslopes bounding the site. Coarse-grained alluvial deposits and fine-grained alluvial overbank deposits are sourced by Green Valley Creek which bounds the site to the south and west (Figure 3). Alluvial deposits were encountered in trenches T1-5 and T7-16 (Figure 3). Moderately coarse-grained slope-derived colluvium was only encountered in one trench, T6, where the trench traversed the west facing bedrock hillslope (Figure 3). Slope-derived colluvium was observed to interfinger with fine-grained overbank alluvial deposits of unit 300 (described below). For trench logs refer to the Final Technical Report submitted to the U. S. Geological Survey National Earthquake Hazards Reduction Program for Award Numbers G10AP00065 and G10AP00064, and event evidence and interpretation published in Streig *et al.*, 2012 *AGU fall meeting abstracts*; Streig *et al., in press BSSA*.

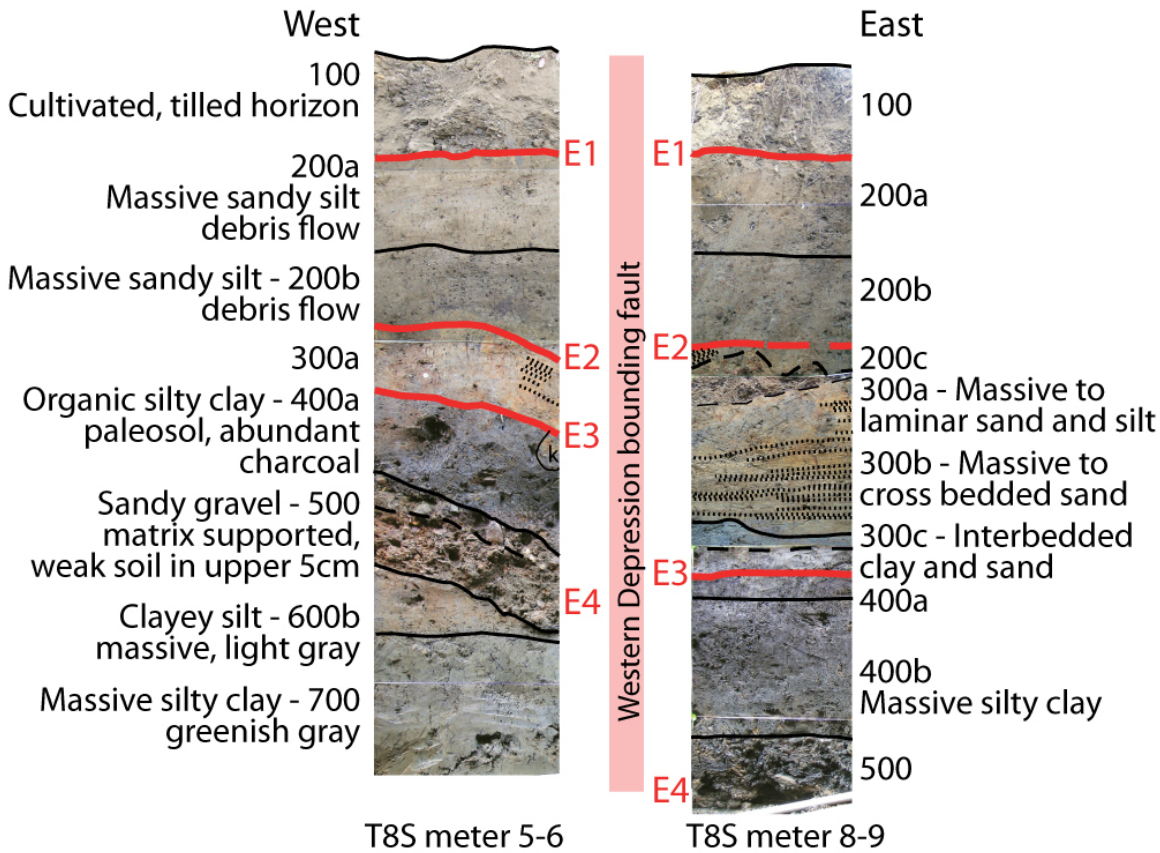

Figure 4. Stratigraphic columns and descriptions of deposits on a photo-mosiac base showing unit correlations west of the depression bounding fault and stratigraphy within the depression. The photo-mosaic is overlain with linework; black lines are unit contacts; shaded lines labeled E1 through E3 are earthquake horizons.

Unit 700 is massive greenish gray clay, observed only west of the structural depression (sag) bounding fault (Figure 4). The base of the unit was not exposed; however as much as 50 to 65 cm of unit thickness is exposed in trenches T8 and T10a. This is the oldest unit observed and correlated between trenches.

Unit 600 is silty clay coarsening upward to silty sand, and is divided into subunits 600a and 600b (Figure 4). 600a is a light gray silty sand to silt, with some brown to strong brown mottles. This unit has a gradational basal contact to unit 600b. Unit 600b is light gray clayey silt to silty clay with common brown to strong brown mottles in the upper 15 cm. the basal contact is sharp over 5 cm, and wavy. Unit 600a is discontinuous, and directly underlies the gravel unit 500. Unit 600a ranges between 10 to 15 cm thickness, where preserved, and unit 600b is 20 – 30 cm thick in trenches T8 and T10a. These units are observed west of the depression-bounding fault, and are correlated between trenches.

Unit 500 is sandy gravel, composed primarily of sand and pebbles, with occasional cobbles, and is the deepest and oldest stratigraphic unit observed both east and west of the fault (Figure 4). Unit 500 is 20 to 35 cm thick west of the fault; the base of the unit was not exposed east of the western sag-bounding fault. This unit unconformably overlies unit 600a and 600b.

Unit 400 is massive gray to black clayey silt with abundant detrital charcoal fragments, it is subdivided into units 400a and 400b. The upper horizon, 400a (15-20 cm) is defined by a distinct dark gray to black color that grades downward to medium grey, it is massive to weakly laminated in areas with redwood needle hash layers and abundant detrital charcoal. 400b is dark gray to gray blue clayey silt with lesser amounts of charcoal. The basal contact of the unit is slightly wavy and gradational over 5 to 10 cm. This unit represents fine-grained overbank alluvial deposits with strong organic soil development in unit 400a, the upper 20 to 30 cm of the deposit, is a buried soil and shows a period of marsh stability prior to deposition of the overlying sandy alluvial unit 300. Unit 400a is 5 cm thick west of the depression-bounding fault, and 8 – 20 cm thick east of the fault (Figure 4).

Unit 300 is light tan to grayish-orange silty sand to sandy silt and consists of three distinct alluvial deposits, subunits 300a, 300b and 300c (Figure 4). Subunit 300c is a massive to finely laminated light grayish yellow silty sand, within the structural depression in trench T10 the unit is interbedded very fine sand, silt and organic debris layers, with some angular axe-cut wood chips at the base of the unit. Unit 300c infills a depression formed on the unit 400a surface. 300c is 20 – 25 cm thick in trenches T7 and T8, and thickens substantially within the depression. At its thickest it is 70 cm in T10a; unit thickness decreased in subsequent cuts northward to 50cm in cut T10f. Historical axe-cut wood chips were found at the base of unit 300c. Subunit 300b is a massive to locally laminated and crossbedded tan to light orange silty sand. Unit 300b ranges from 15 to 30 cm thickness in all trench exposures. This is overlain by unit 300a, massive sandy silt to silty sand with some fine laminations. Unit 300a has a sharp to diffuse and planar basal contact, is 10 to 25 cm thick, and is not preserved everywhere. Units 300a, b and c represent relatively low-energy water-lain and marsh deposits (Figure 4).

Unit 200 is light gray to grayish brown massive clayey silt with sand to coarse sand layers and consists of subunits 200a, 200b, 200c, 200d and 200f (Figure 4). Unit 200a is light grayish brown silt, well sorted and massive, and is 10 – 25 cm thick. Subunit 200b is massive, contained abundant roots and rootlets and has a relatively planar basal contact that is gradational over roughly 5 cm, and is 15 – 30 cm thick. Subunit 200a conformably overlies subunit 200b and grades upward from sandy silt to clayey silt with sand, the basal contact is gradual over ~5 cm. Unit 200c is massive, poorly sorted silt to coarse sand, this unit grades into 200d which has pockets of grain-supported coarse sand along the base. Unit 200c is 35 cm thick in trench T10, and tapers to the north and south to 25 cm thickness in T7 and T8. Unit 200d is only observed in trench T10 cuts A through F, and is 15 – 30 cm thick. Unit 200f is a medium to dark gray brown massive silty sand with a weak incipient soil. 200f is only observed in trench T10 A through F, and is 5 – 10 cm thick. Unit 200 reveals a depositional change from well-sorted laminated sands and interbedded silts, clays and organic layers of Units 300a, 300b and 300c, to higher energy, coarse grained, massive mud flow deposits of Unit 200. Unit 200f reveals that there was a brief hiatus in deposition of the unit 200 sequence, 200f was deposited and persisted at the surface long enough to develop a weak soil, then was subsequently buried by 200d through 200a.

Unit 100 represents agriculturally modified stratigraphy immediately below the ground surface including the depth of the till-zone and roots from former apple trees. This unit ranges from 30 to 40 cm thickness, and has a sharp (over 1 - 2 cm) wavy basal contact.

2.3 Event Chronology at the Hazel Dell site

We find evidence of four earthquakes, and enough exposure to suggest that there is a complete record since the formation of a buried soil on unit 400a, recording the last three earthquakes (E1, E2 and E3; Streig *et al.*, 2012). While the evidence for E4 is clear, the lack of stratigraphic section between E3 and E4 makes it impossible to rule out additional events or the possibility that "E4" combines evidence for more than one event.

Event E1 – 1906: Evidence for the most recent event, E1, the 1906 rupture, is expressed in trenches 7 and 8 as one to two fault strands that extend upward to the base of unit 100, or terminate within unit 200a, the upper mudflow unit, in some exposures (Figure 4).

Event E2: The penultimate earthquake and E3 occur on more easterly fault traces than E1. Event E2 places unit 200c and 200d in vertical fault contact with unit 300a and b; this relationship was exposed in multiple cuts of trench 10. E2 fault traces do not extend upward into 200a, and often do not clearly extend up into 200b (Figure 4).

Event E3: Earthquake E3 occurred when the top of unit 400a was the ground surface. Axe-cut wood chips are incorporated in the upper few centimeters of unit 400a and scattered near the base of the overlying sequence 300c (Figure 4).

Event E4: Evidence for the oldest event (or possibly events; in either case we refer to all evidence at this horizon as E4) was identified in trenches T8 and T4. E4 is expressed as upward fault terminations within the oldest gravel unit 500b, and as upward terminating fissures which contain gravels from the overlying unit, 500b, in the fissure fill (Figure 4).

2.4 Methods

The site revealed fine-grained stratigraphy, historical axe-cut wood chips (Figure 5), an abundance of datable material, including Wood chips, plant material and detrital charcoal that were collected from stratigraphic units in the field. We collected oriented block samples of units 300 and 400, and the contact between these units with the goal of improving the resolution of age dates for these units by dating macrofossils collected from organic-hash layers interbedded with silt. Using a binocular microscope we examined scrapings from stratigraphic block samples from unit 300a, b, c and d, and unit 400a for the presence of macrofossils (Figure 6). We identified and collected redwood needles, redwood branches, redwood cones, seeds and detrital charcoal from the scrapings (Figure 6). These samples were ranked based on the sample type, size and the location within the unit from which they were recovered, and were prioritized for ^{14}C analysis.

Figure 5. Examples of wood chips collected from unit 400a. A) Transverse cut across wood grain. Larger sample, 10 cm wide by 20 cm long. B) Smaller wood chip with very fine ~1 to 2 mm wide cuts at opposing angles suggests narrow-bladed steel axe. C) Wood chip with bark, 180 growth rings, inner and outer rings were sampled and used in 14C analysis, sample HD-2011-WC1. D) Wood chip with bark, 24 growth rings, inner and outer rings were sampled and used in 14C analysis, sample HD-2011-WC2.

Axe-cut redwood chips were collected from the upper few centimeters of unit 400a, and within the base of unit 300c. The wood chips range in size from a few centimeters to >20 cm length. All wood chips collected at this horizon have very sharp, angular cuts

transverse to the wood grain. These very sharp cuts reveal that the wood has not been transported a significant distance and is well preserved in its original cut shape. There are no known ethnographic or historical accounts of pre-contact native people chopping down large trees in the way that European colonists would have. Local indigenous populations didn't make large hafted axes needed to cut large trees (Anderson, 2005; Lightfoot *et al*., 2009). Redwood lumber harvest began in this area sometime around or before 1832, "Amesti is said to have had a whipsaw lumber mill in 1832 on the upper Corralitos ." (http://www.corralitoshistory.com/additions.html, on 1/20/2010). The timing of this lumber mill indicates that the earthquakes E2 and E3 are historical.

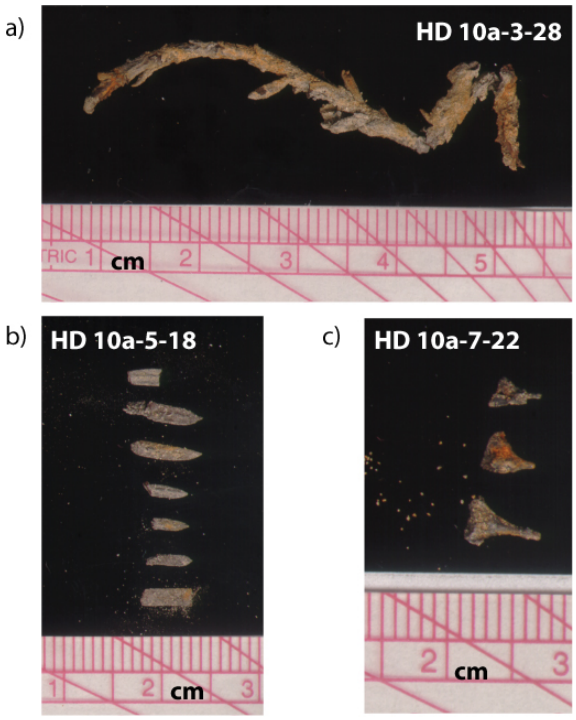

Figure 6. Photographs of macro fossils collected from block stratigraphic samples. Sample numbers represent the site, trench number, stratigraphic block sample number, and macrofossil sample number from scrapings of that block. For example, HD 10a-3-28 is collected from trench T10a, block sample 3, macrofossil sample # 28. a) Sample HD 10a-3-28. Redwood branch and needles, collected from a key stratigraphic contact at the top of unit 400a and the base of unit 300c. b) Sample HD 10a-5-18, Redwood needles. Collected from unit 300c. c) Sample HD 10a-7-22, Redwood cone fragments. Collected from unit 300c. Radiocarbon age dates for these samples are reported in Table 1.

3.0 RESULTS

3.1 Radiocarbon Analysis

We sampled organic material from stratigraphic units 300 and 400 for accelerator mass spectrometry (AMS) ^{14}C age determination. Wood, redwood needles, redwood cone fragments and some charcoal samples were analyzed at the Center for Accelerator Mass Spectrometry (CAMS) at Lawrence Livermore National Laboratory (LLNL). Detrital charcoal samples collected in the first year of the study (2008) were submitted to Beta Analytic Inc., Florida. Each sample was pretreated with acid-alkali-acid washes and results are reported as conventional radiocarbon ages (years B.P.) in Table 1.

We cut wood samples from inner and outer growth rings on two of the wood chips that had preserved bark (Figure 5c, d), and obtained and AMS ^{14}C age distributions in conventional radiocarbon years before present (BP) for the annual growth rings (Table 1). These AMS radiocarbon ages have uncertainties on the order of three to four decades (Table 1). ^{14}C age calibration using OxCal 4.1 (Bronk Ramsey, 2009) for these samples yields broad calendaric ages ranges, often with multi-peaked age distributions, and with statistical uncertainty on the order of several decades. We use a technique known as 'wiggle-matching', that uses the known interval (years) between growth ring samples and the ^{14}C calibration curve, to yield more exact calibrated calendar ages. The wood chips were selected based on the presence of preserved bark on the sample, meaning that we were able to sample the outer rings, as well as the inner-most ring preserved on the sample, providing a growth period of 180 years for sample HD-2011-WC-1 and 24 years for sample HD-2011-WC-2 (Figure 5). The bark indicates that the outer growth ring is in place, and so would give an age close to the death of the tree. However, redwood has notoriously irregular growth, including discontinuous growth rings and areas with concentrated growth hormone and abundant more continuous growth rings (Fritz, 1940). As a result there can be a lot of variability on the age of the outer growth ring around the stem. The woodchips we've sampled could be from anywhere on the tree, and the outer ring on the wood chips may not contain growth rings from the last growth year of the tree. For this reason we are in the process of analyzing a continuous growth transect of a redwood stump (Section 3.3).

^{14}C dates with the relative age between samples (years determined by counting the number of growth rings) were 'wiggle-matched' with the intercepts of the IntCal 04 and 98 terrestrial ^{14}C calibration curve (Figure 7, 8; Reimer *et al.*, 2004). The IntCal 04 and 98 calibration curves show fluctuation of ^{14}C concentration of atmospheric CO_2 over the last 500 years BP (where BP is the calendar year1950 AD). Changes in ^{14}C production rate result from modulation of intensity of cosmic rays entering the earth's atmosphere and also by variations of geomagnetic intensity and solar activity (Reimer *et al.*, 2004). Trees take up atmospheric CO_2 in photosynthesis and so record temporal variations of ^{14}C in their growth rings. Fluctuations of ^{14}C abundance for the last 12,400 years has been mapped out with precisely dated transects of annual growth rings from trees in North America and Europe (Reimer *et al.*, 2004). We employ the ^{14}C 'wiggle matching' technique for the wood chips, and plot the measured ^{14}C ages (^{14}C BP) for successive growth rings on the plot of ^{14}C fluctuations shown by the IntCal04 and 98 calibration

data. We know the annual interval between samples from the growth ring count, and shift the paired samples on the axis for calibrated calendar age (X-axis on Figures 7 and 8) until we get the best fit to the IntCal04 and 98 data, within error of the measured ^{14}C ages (technique of Nakamura *et al.*, 2007).

Wood chip HD-2011-WC-1 had 180 growth rings and spans a distinct peak and trough in ^{14}C abundance on the IntCal04 calibration curve (Figure 7). The inner growth ring, HD-2011-WC-1A, yielded a radiocarbon age of 280 ± 30 ^{14}C yrs BP and has only one intercept with the ^{14}C calibration curve (Figure 7). The ^{14}C age for the inner growth ring also falls on a steep part of the ^{14}C calibration curve, giving a narrow range of calendric ages (Figure 7). The outer growth ring, HD-2011-WC-1B yielded a measured age of 130 ± 40 ^{14}C yrs BP, and has only one intercept with the calibration curve that fits the known interval of 180 years between samples (Figure 7). Sample HD-2011-WC-1B falls on a steep part of the calibration curve, also minimizing the span of calendar ages for this sample. Using the age of the outer-growth ring constrained by the age of the inner growth ring and the interval between these samples, we find that the outer growth ring of woodchip HD-2011-WC-1 predates 1813 AD. This date is the latest possible intercept of the ^{14}C age for the outer growth ring (HD-2011-WC-1B, Figure 7) with the calibration curve.

We find that to confidently use the wiggle-matching technique the interval between samples should span more than two decades, and ideally at least one of the samples should fall onto steep and distinct portion of the calibration curve, which minimizes the range of calendar years BP, and ideally more than two growth rings should be analyzed. For this reason we have more conclusive results with woodchip sample HD-2011_WC1, which had 180 years between samples. Woodchip HD-2011-WC-2 did not yield such conclusive results, this sample had 24 growth rings, and the time interval between rings was less than the uncertainty of the measured ^{14}C age for both AMS samples. Additionally, the measured ^{14}C dates for woodchip HD-2011-WC-2 had two or more intercepts with the calibration curve. The inner growth ring, sample HD-2011-WC-2A yielded a radiocarbon age of 115 ± 30 ^{14}C yrs BP, and intercepts the calibration curve in four places. We can exclude intercepts for the inner growth ring, sample HD-2011-WC-2A that post date the range of possible ages for the outer growth ring (Figure 8). The outer ring HD-2011-WC-2B yielded a radiocarbon age of 185 ± 35^{14}C yrs BP, and must post-date the inner ring by at least 24 years. The ^{14}C date for the outer ring has only two intercepts with the calibration curve, we deduce that the tree must have died before 1810 AD, the latest possible calendar date for the outer growth ring (Figure 7). Lastly, we plotted ^{14}C radiocarbon ages for macrofossils, samples HD10a-3-28, HD10a-5-18 and HD10a-7-22 against the IntCal 04 calibration curve, and find that the dates for these macrofossils cluster around the calibration curve peak at 1800 AD (Figure 9), and coincide with the age for the death of the tree using the wiggle-match technique.

Additionally, we use a Bayesian statistical approach combining14C dates from inner and outer growth rings with the relative age between samples (years determined by counting the number of growth rings) was employed to wiggle-match the results using OxCal v.4.1.7 (Bronk Ramsey, 2012; Bronk Ramsey et al., 2001). Using their wiggle-matching technique OxCal yields a 2σ modeled felling age range of 1698 to 1850 for sample HD_2011_WC1, and 1725 to 1973 for sample HD_2011_WC2. The OxCal modeled

felling dates for wood chips HD-2011-WC-1 and HD-2011-WC-2 are shown in Figures 7 and 8.

Table 1 - Radiocarbon Ages for wood chips, redwood cones & needles, and detrital charcoal from the Hazel Dell Site.

Sample Name	Laboratory Number [a]	Unit	^{14}C age [b, c]	±	Material
HD T7-2	Beta-264162	200b	220	40	Charcoal
HD T7-7	Beta-254277	200b	350	40	Charcoal
HD T7-3	Beta-254274	300a	1150	40	Charcoal
HD10a-5-18	CAMS-158276	300c	220	30	Redwood needles
HD10a-7-22	CAMS-158277	300c	230	30	Redwood cone fragments
HD T8-2	Beta-264164	300c	340	40	Charcoal
HD10a-3-28	CAMS-158278	400a Top/300c base	190	30	Redwood branch and needles
HD10a-3-28-duplicate	CAMS-158289	400a Top/300c base	160	30	Redwood branch and needles
HD-2011-WC-1-A	CAMS-158281	400a Top	280	30	Wood chip, inner growth ring
HD-2011-WC-1-B	CAMS-158282	400a Top	130	40	Wood chip, outer growth ring
HD-2011-WC-2-A	CAMS-158283	400a Top	115	30	Wood chip, inner growth ring
HD-2011-WC-2-B	CAMS-158284	400a Top	185	35	Wood chip, outer growth ring
HDT8-40-1	CAMS-158280	400a	350	30	Charcoal
HD T7-5	Beta-264163	400a	340	40	Charcoal
HD T7-1	Beta-264161	400a	590	40	Charcoal
HD T7-4	Beta-254275	400a	650	40	Charcoal
HD T7-6	Beta-254276	400a	640	40	Charcoal
HD T8-31	Beta-254278	600b	1250	40	Charcoal
HDT8-32-2008	CAMS-158279	600b	1270	30	Charcoal
HD 4-1	Beta-264157	700a Top	2260	40	Charcoal
HD 4-7	Beta-264158	700b Base	2120	40	Charcoal
HD 4-9	Beta-264159	700b Base	2300	40	Charcoal
HD 4-12	Beta-264160	900	2710	40	Charcoal

Notes:

a) Samples processed at Center for Accelerator Mass Spectrometry (CAMS) at Lawrence Livermore National Laboratory and Beta Analytic Inc., Florida (Beta).

b) The quoted age is in radiocarbon years using the Libby half life of 5568 years and following the conventions of Stuiver and Polach (ibid.).

c) Radiocarbon concentration is given as conventional radiocarbon age.

d) Sample preparation backgrounds have been subtracted, based on measurements of samples of ^{14}C-free wood.

Note: Backgrounds were scaled relative to sample size.

(a) Wiggle-match Plot of 14C dates for Wood Chip Sample WC-1

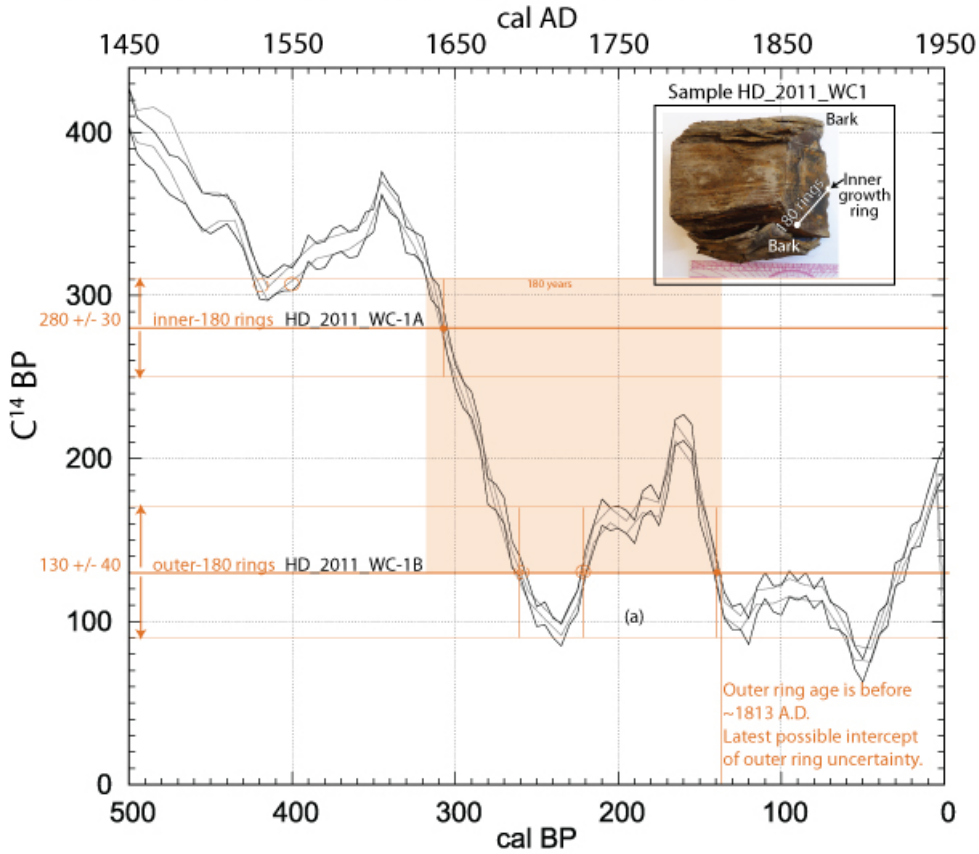

(b) Wiggle-match OxCal Model for Wood Chip Sample WC-1

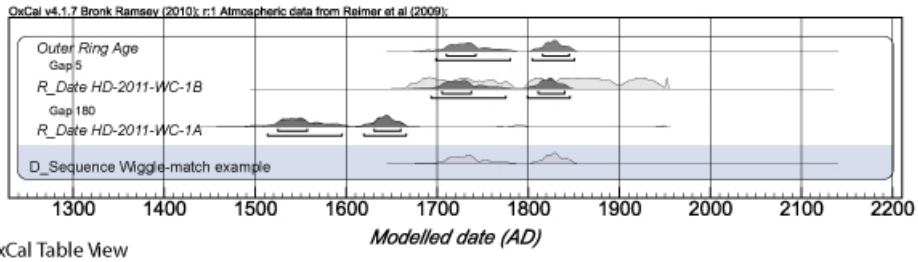

OxCal Table View

Name	Unmodelled (BC/AD) from	to	%	from	to	%	Modelled (BC/AD) from	to	%	from	to	%	Indices A_{comb}	A
Outer Ring Age							1710	1845	68.2	1698	1850	95.4		
R_Date HD_2011_WC_1B	1682	1952	68.2	1669	1953	95.3	1705	1840	68.2	1693	1845	95.4		100.4
R_Date HD_2011_WC_1A	1524	1659	68.2	1496	1795	95.4	1525	1660	68.2	1513	1665	95.4		104.7
▲ D_Sequence Wiggle-match	1710	1845	68.2	1698	1850	95.4								103.6

Figure 7. a) Plot of ^{14}C dates for inner and outer growth rings for woodchip HD_2011_WC1 samples 1A (inner ring) and 1B (outer ring) with the IntCal ^{14}C calibration curve. IntCal 98 (gray lines) and IntCal 04 (black lines) 1 – standard deviation error envelopes for 0 – 500 cal BP (Reimer et al., 2004). **b)** OxCal modeled outer growth ring age range for wood chip HD-2011-WC-1 and OxCal Table for sample HD-2011-WC-1. A Bayesian approach combining 14C dates from inner and outer growth rings with the relative age between samples (years determined by counting the number of growth rings) was employed to wiggle-match the results using OxCal v.4.1.7 (Bronk Ramsey, 2012; Bronk Ramsey et al., 2001). Using their wiggle-matching technique OxCal yields a 2σ modeled outer ring age range of 1698 to 1850. Prior Probability distribution functions (pdf's) for radiocarbon samples shown in light gray, posterior pdf's shown in dark gray for samples.

(a) Wiggle-match Plot of 14C dates for Wood Chip Sample WC-1

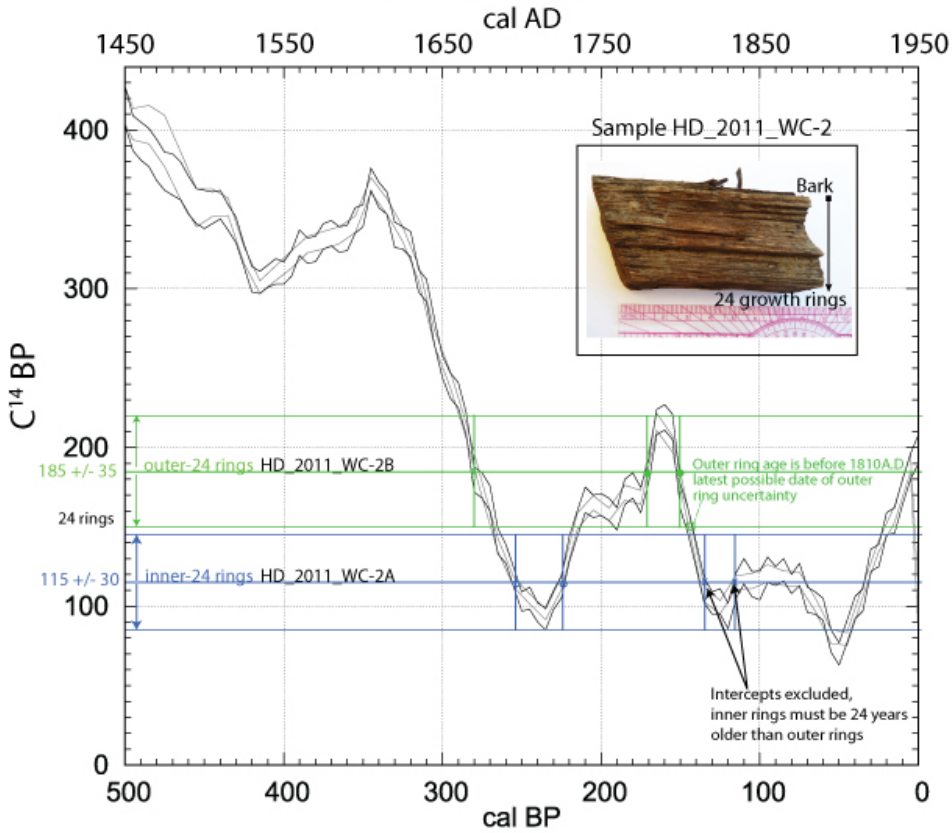

(b) Wiggle-match OxCal Model for Wood Chip Sample WC-2

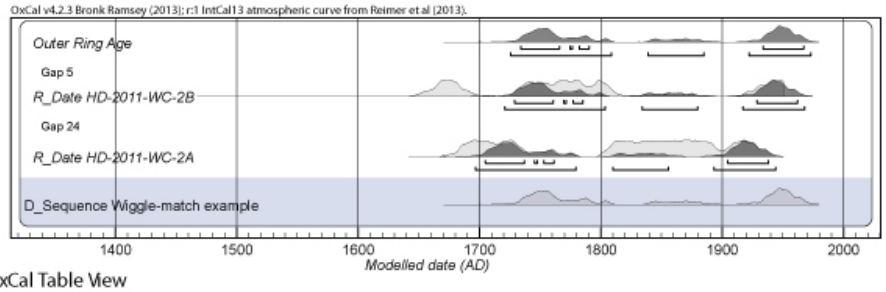

OxCal Table View

Name	Unmodelled (BC/AD) from	to	%	from	to	%	Modelled (BC/AD) from	to	%	from	to	%	Indices A_{comb}	A
Outer Ring Age							1734	1967	68.3	1725	1973	95.3		
R_Date HD-2011-WC-2B	1664	....	68.3	1649	...	95.4	1729	1962	68.3	1720	1968	95.3	100.3	
R_Date HD-2011-WC-2A	1690	1925	68.2	1680	1938	95.5	1705	1938	68.3	1696	1944	95.3	89.7	
▲ D_Sequence Wiggle-match	1734	1967	68.3	1725	1973	95.3							92.8	

Figure 8. a) Plot of ^{14}C dates for inner and outer growth rings for woodchip HD-2011-WC-2 samples 2A (inner ring) and 2B (outer ring) with the IntCal ^{14}C calibration curve. IntCal 98 (gray lines) and IntCal 04 (black lines) 1 – standard deviation error envelopes for 0 – 500 cal BP (Reimer et al., 2004). **b)** OxCal outer growth ring age range for wood chip HD-2011-WC-2 and OxCal Table for sample HD-2011-WC-2. A Bayesian approach combining 14C dates from inner and outer growth rings with the relative age between samples (years determined by counting the number of growth rings) was employed to wiggle-match the results using OxCal v.4.1.7 (Bronk Ramsey, 2012; Bronk Ramsey et al., 2001). Using their wiggle-matching technique OxCal yields a 2σ modeled outer ring age range of 1725 to 1973. Based on our paleoseismic data, we know that the outer growth ring of these wood chips grew before the 1906 earthquake. This information trims the felling age range for sample HD_2011_WC2, from the 2σ modeled age range of 1725 to 1973 to 1725 to 1906. Prior Probability distribution functions (pdf's) for radiocarbon samples shown in light gray, posterior pdf's shown in dark gray for samples.

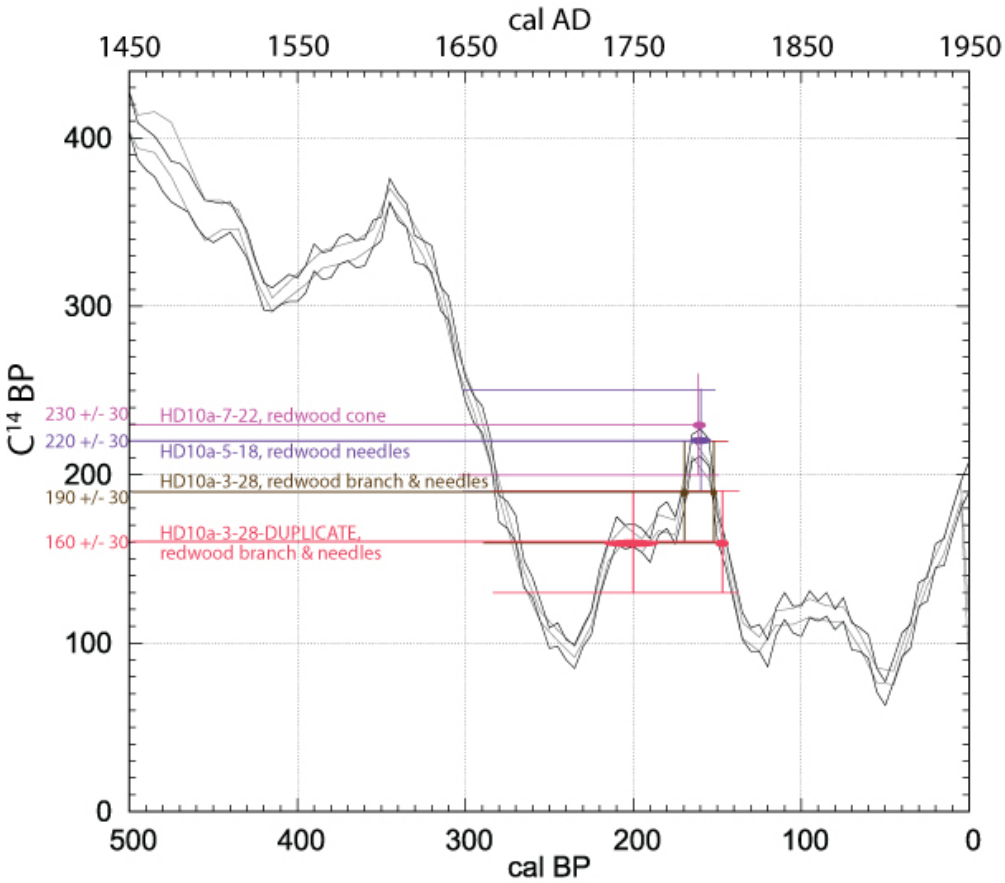

Figure 9. Plot of macrofossil ^{14}C dates with the IntCal ^{14}C calibration curve. Sample HD10a-7-22 shown as pink point, are fragments of a redwood cone. Sample HD10a-5-18 shown by the purple point is a date from redwood needles. Sample HD10a-3-28 shown in brown is a redwood branch or twig and needles, and sample HD10a-3-28DUPLICATE is a duplicate sample run of the redwood branch and needles. IntCal 98 (gray lines) and IntCal 04 (black lines) 1 – standard deviation error envelopes for 0 – 500 cal BP (Reimer et al., 2004). These samples cluster around 1800. The earlier intercept at 1750 AD for sample HD10a-3-28-Duplicate (shown in pink) is not possible given the age ranges of the wood chips, we prefer the second intercept at 1800.

Detrital charcoal samples and macro-fossils were reviewed, and prioritized for radiocarbon dating based on sample size, shape (angularity) and location (proximity to upper or lower contact). Fifteen detrital charcoal samples from key stratigraphic units were submitted for radiocarbon analysis (Table 1). Of these samples, eight were in good stratigraphic order, and seven samples were inconsistent with ages determined from both overlying and underlying samples and are not included in our OxCal age model (Figure 10). Probability distribution functions for radiocarbon ages are shown in stratigraphic order in Figure 10.

We use these radiocarbon ages and historic constraints, like the timing of the 1906 earthquake, to build an age model and estimate age distributions for earthquakes E2 - E4 using OxCal v. 4.1.7 (Figure 10; Bronk Ramsey, 2009).

3.2 Earthquake Age Estimates

We interpret E1, the most recent event at Hazel Dell, to be the 1906 rupture, based on historical accounts of the earthquake rupturing through the Santa Cruz Mountains to the vicinity of San Juan Bautista (Prentice and Schwartz, 1991). Based on the historical constraints from the cut wood chips, we have two additional historical earthquakes that occurred in the 19th century and with these constraints, the OxCal modeled age for E2 is 1840 to 1906 (2σ uncertainty, Figure 10), and the OxCal modeled age for E3 is between A.D. 1815 and 1895. E4, our oldest paleoearthquake is prehistoric with a modeled age with 2σ uncertainties between A.D. 760 – 1318 (Figure 10).

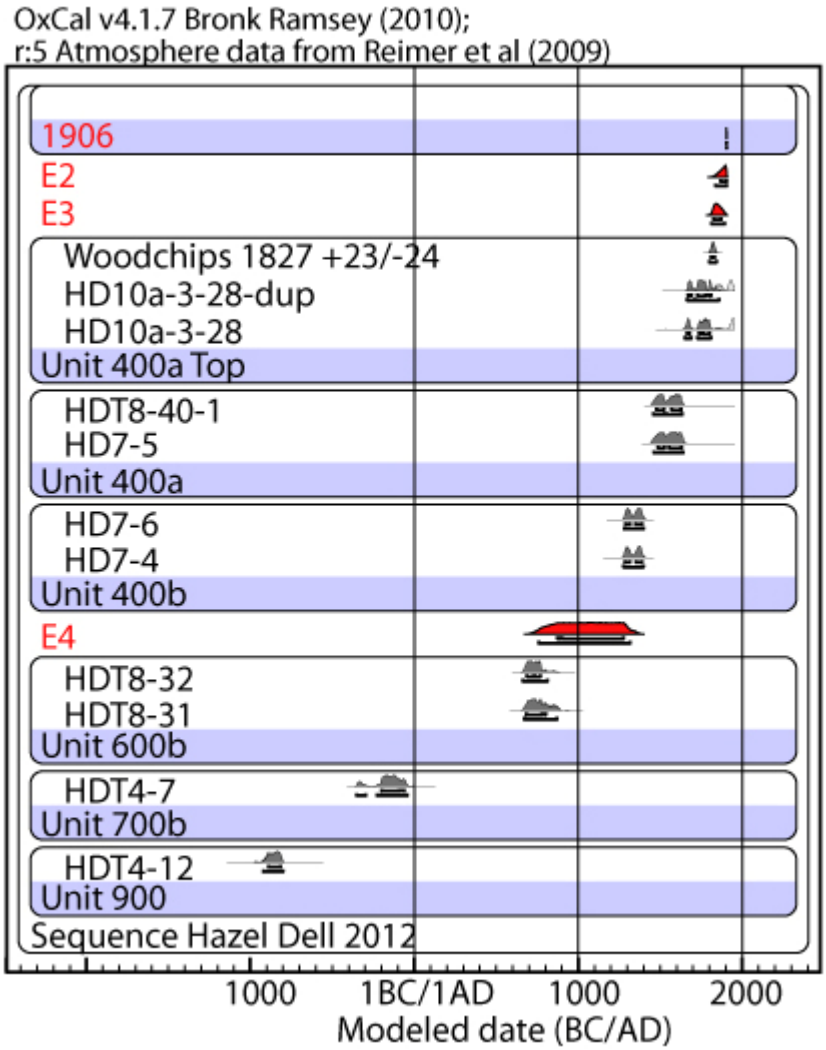

Figure 10. OxCal model of stratigraphic ages constraining the timing of earthquake horizons at the Hazel Dell site. Prior probability distribution functions (pdf's) for radiocarbon samples shown in light gray, posterior pdf's shown in dark gray. Unit numbers shown on the shaded bars. Modeled earthquake ages are labeled by event name. Note – inconsistent samples removed, see Table 1 for complete list of samples.

3.3 Improving Age Estimates: Wiggle-matching a redwood tree stump

To improve the age resolution for the onset of logging at the site we excavated and cut a slab from an *in situ* redwood tree stump rooted in the E3 horizon, unit 400a. The redwood stump was encountered during 2008 excavations at the intersection of trenches T1 and T6 (Figure 3). In 2012 we exposed two stumps growing together with a combined length of roughly 1.75 meters (Figure 11a). We cut a roughly 25cm thick slab from the smaller stump, measuring 60 cm diameter for tree ring analysis (Figure 11a, b). We collected the smaller stump because it had continuous growth rings, the larger stump had burnt and gouged areas and wouldn't have yielded a continuous cross section and so would have been useless for our wiggle-matching purposes. We sanded and polished the slab to count the annual growth rings along a cross section (Figure 11). We counted 274 rings, counting from the pith (inner growth ring) outward. We marked decades, 50th year and century years on the cross section (Figure 11c). We collected and ran samples from 14 growth rings spanning from the pith to the outer growth ring. Samples were analyzed at the Center for Accelerator Mass Spectrometry (CAMS) at Lawrence Livermore National Laboratory (LLNL) for AMS ^{14}C age determination (Table 2). Pending ^{13}C measurements, we find that the youngest ring we have identified in the tree is A.D. 1800.

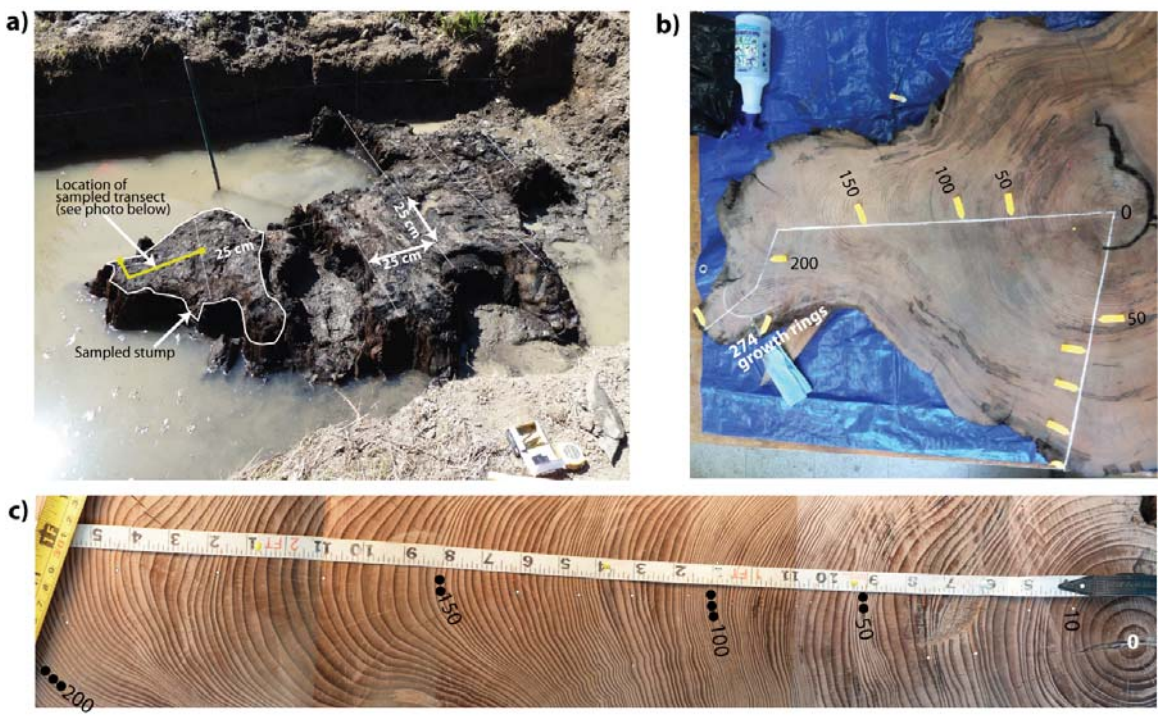

Figure 11. Buried redwood tree stump excavated during 2012 field season, this stump was located at the intersection of trenches T1 and T6, shown in Figure 3. a) photograph of two buried stumps *in situ*, excavated during summer 2012. A slab of the stump outlined in white, on the left side of the photo, was collected. b) Sanded slab of tree stump. Annual growth rings are shown along two white transects. The innermost ring, the pith, is shown as zero, and the outermost ring we identified was 274. Growth rings were correlated around the stump and are shown by yellow arrows in increments of 50. c) Photograph of polished transect, along the longer transect line shown in the center of photo b. Early wood is light in color, late wood is dark in color and shows the end of an annual growth ring. The ruler shows distance in inches along the cross section from 0 to 200 growth rings. Centuries are shown by three black dots, fifty year increments are shown by two dots, and decades are shown as small white dots.

Upon receiving ^{13}C measurements we will wiggle match 14 radiocarbon dates sampled from annual growth rings taken from the stump and the known interval between growth rings, with the intercepts of the IntCal 04 terrestrial ^{14}C calibration curve.

Table 2 - Preliminary Radiocarbon Ages for annual growth rings collected from a redwood stump at the Hazel Dell Site.

Sample Name	Laboratory Number [a]	^{14}C age [b, c, d]	±	Material	Growth Ring (1 = pith, 274 outer most ring)
HD2013_S1	161669	350	20	Growth ring. Redwood, tree stump	Ring 1, innermost ring. Pith.
HD2013_S1 duplicate	161670	350	20	Growth ring. Redwood, tree stump	Ring 1, innermost ring. Pith.
HD2013_S40	161671	330	20	Growth ring. Redwood, tree stump	Ring 40
HD2013_S50	161672	330	20	Growth ring. Redwood, tree stump	Ring 50
HD2013_S50 duplicate	161673	365	20	Growth ring. Redwood, tree stump	Ring 50
HD2013_S60	161674	350	20	Growth ring. Redwood, tree stump	Ring 60
HD2013_S60 duplicate	161675	370	20	Growth ring. Redwood, tree stump	Ring 60
HD2013_S70	161676	365	20	Growth ring. Redwood, tree stump	Ring 70
HD2013_S80	161677	360	20	Growth ring. Redwood, tree stump	Ring 80
HD2013_S80 duplicate	161678	335	20	Growth ring. Redwood, tree stump	Ring 80
HD2013_S90	161679	365	20	Growth ring. Redwood, tree stump	Ring 90
HD2013_S100	161680	375	20	Growth ring. Redwood, tree stump	Ring 100
HD2013_S130	161681	285	20	Growth ring. Redwood, tree stump	Ring 130
HD2013_S140	161682	210	20	Growth ring. Redwood, tree stump	Ring 140
HD2013_S150	161683	215	20	Growth ring. Redwood, tree stump	Ring 150
HD2013_S150 duplicate	161684	180	20	Growth ring. Redwood, tree stump	Ring 150
HD2013_S170	161685	190	20	Growth ring. Redwood, tree stump	Ring 170
HD2013_S170 duplicate	161686	145	20	Growth ring. Redwood, tree stump	Ring 170
HD2013_S240	161687	145	25	Growth ring. Redwood, tree stump	Ring 240
HD2013_S240 duplicate	161688	155	20	Growth ring. Redwood, tree stump	Ring 240
HD2013_S271	161689	730	20	Growth ring. Redwood, tree stump	Ring 271,near bark.
HD2013_S271 duplicate	161690	260	20	Growth ring. Redwood, tree stump	Ring 271,near bark.

Notes:

a) Samples processed at Center for Accelerator Mass Spectrometry (CAMS) at Lawrence Livermore National Laboratory

b) Preliminary 14C ages, a d13C value of -22 was used as the assumed value for all samples according to Stuiver and Polach (Radiocarbon, v. 19, p.355, 1977).
Final results pending laboratory measured δ13C values for each sample.

c) The quoted age is in radiocarbon years using the Libby half life of 5568 years and following the conventions of Stuiver and Polach (ibid.).

d) Radiocarbon concentration is given as conventional radiocarbon age.

e) Sample preparation backgrounds have been subtracted, based on measurements of samples of ^{14}C-free wood.
Backgrounds were scaled relative to sample size.

4.0 SIGNIFICANCE OF RESULTS

The Hazel Dell site, on the Santa Cruz section of the San Andreas fault (SAF), has yielded good evidence of the 1906 surface rupture, and three earlier earthquakes in the form of filled fault bounded depressions, upward terminations of fractures, and stratigraphic thickness changes related to ground surface deformation. Evidence for E1, the 1906 earthquake, consists of faults that extend to the base of unit 100, a unit characterized by bioturbation and agricultural use. Evidence for the penultimate event, E2, is expressed as upward fault terminations within a massive sand infilling a topographic low. This sand was deposited within a depression formed by the pre-penultimate earthquake, E3. E3 formed a roughly 7 meter long and 1.5 meter wide oblong structural depression, or sag, with as much as 1.5 meters vertical relief at the apex of the sag. The depression extends between trenches 7 and 8.

We identified steel blade cut wood chips stratigraphically coincident with the pre-penultimate earthquake horizon, which suggests that surface rupturing earthquake E2 occurred after deposition of the milled wood stratigraphic unit, and E3 occurred either immediately after the wood chips were deposited on the surface. Logging began in this area sometime around or before 1832, these units were deposited after lumber harvesting began in the area which suggests that earthquakes E2 and E3 are historical. To improve this age constraint we ran C^{14} samples for two wood chips collected from the E3 horizon. We wiggle match these results with the IntCal 04 calibration curve and find that the wood chips were cut after 1810-1813 AD. We also collected redwood needles, branches, and redwood cone fragments from the stratigraphic sequence infilling the graben formed by E3. AMS C^{14} ages for these samples are consistent with the estimated felling date determined from the axe-cut woodchips. Lastly, we excavated a buried redwood stump rooted in the E3 earthquake horizon and ran C^{14} dates for 14 annual growth rings, and will use these results to better constrain the onset of logging at the site. These refined age constraints for earthquakes E2 and E3 suggest more frequent surface rupturing earthquakes on the Santa Cruz Mountains section of the San Andreas fault within historical time than previously recognized.

5.0 ACKNOWLEDGEMENTS

The authors would like to thank the property owner David Dent for allowing us to work on his property and for his continued interest in our results. We thank Carol Prentice, David Schwartz, Suzanne Hecker, Gordon Seitz, Ron Rubin, Andy Lutz and Steve Thompson for their thoughtful field review and insightful discussion of event evidence. We thank Rachel Lippoldt, Courtney Streig, Nyle Weldon and Spencer Kendall for their assistance in the field.

6.0 REFERENCES

Bakun, W.H., 1999, Seismic Activity of the San Francisco Bay Region, Bull. Seism. Soc. Am, 89, 764-784.

Bronk Ramsey, C., 2009, OxCal Program, v.4.1.3, Radiocarbon Accelerator Unit, University of Oxford, Oxford, United Kingdom, https://c14.arch.ox.ac.uk/oxcal.html (last accessed on December 2011).

Brabb, E.E., 1989, Geologic map of Santa Cruz County California, scale 1:62,500; *USGS Open-File Report 97-489*, Geologic map of Santa Cruz County California: A digital database prepared by Graham, S., Wentworth, C., Knifong, D., Graymer, R., Blissenbach, J., 1997.

Fritz, E., 1940, Problems in dating rings of California Coast Redwood, Tree-Ring Bulletin, vol. 6, no. 3, pg. 19-22.

Fumal, T.E., 2012, Timing of Large Earthquakes during the Past 500 Years along the Santa Cruz Mountains Segment of the San Andreas Fault at Mill Canyon, near Watsonville, California, Bull. of Seismological Soc. of America, v. 102, doi:10.1785/0120110161.

Fumal, T.E. Heingartner, G.F. Samrad, L., Dawson, T.E., Hamilton, J.C., and Baldwin, J.N., 2003, Photomosaics and Logs of Trenches on the San Andreas Fault at Arano Flat near Watsonville, California: U.S. Geological Survey Open-File Report 03-450, Version 1.0

Hall, N.T., Wright, R.H., and Clahan, K.B., 1999, Paleoseismic studies of the San Francisco peninsula segment of the San Andreas fault zone near Woodside, California: Journal of Geophysical Research, v. 104, no. B10, p. 23,215-23,236.

Johanson, I.A., and Bürgmann, R., 2005, Creep and quakes on the northern transition zone of the San Andreas fault from GPS and InSAR data: Geophysical Research Letters, v. 32, L143056, doi: 10.1029/2005GL023150.

Prentice, C.S., Crosby, C. J., Whitehill, C. S., Arrowsmith, J R., Furlong, K. P., and D. A. Phillips, 2009, GeoEarthScope LiDAR illuminates northern California's active faults, *EOS Transactions of the American Geophysical Union*, **90**, no. 7, p. 55.

Sarna-Wojcicki, A.M., Pampeyan, E.H., and Hall, T.N., 1975, Map showing recently active breaks along the San Andreas fault between the Central Santa Cruz Mountains and the Northern Gablian Range, California: U.S. Geological Survey Miscellaneous Field Studies Map, 1:24,000, Map MF-650.

Schwartz, D.P., Pantosti, D., Okumura, K., Powers, T., and Hamilton, J., 1998, Paleoseismic investigations in the Santa Cruz Mountains: Implications for the recurrence of large magnitude earthquakes on the San Andreas Fault: Journal of Geophysical Research, v. 103, p. 17,985-18,001.

Streig, A.R., Dawson, T.E., and R.J. Weldon, II, *in press September 2013*, Paleoseismic evidence of the 1890 and 1838 earthquakes on the Santa Cruz Mountains Section of the San Andreas Fault, near Corralitos, CA, *Bulletin of the Seismological Society of America, submitted 1/9/2013.*

Streig, A.R., Dawson, T.E., and R.J. Weldon II, 2012, Determining Earthquake Recurrence and Slip Over the Past 3 - 4 events on the Southern Santa Cruz Mountains Segment of the San Andreas Fault: Collaborative Research between Geological Sciences, University of Oregon and the California Geological Survey, Award G10AP00065 and G10AP00064, U.S. Geological Survey Final Report, http://earthquake.usgs.gov/research/external/research.php

Toppozada, T.R., and Borchardt, G., 1998, Re-evaluation of the 1836 "Hayward Fault" earthquake and the 1838 San Andreas Fault earthquake: Seismological Society of America Bulletin, v. 88, p. 140-159.

Toppozada, T.R., Branum, D.M., Reichle, M.S., and C.L. Hallstrom, 2002, San Andreas Fault Zone, California: M ≥ 5.5 Earthquake History, Bull. Seism. Soc. Am, 92, 2555-2601.

Toppozada T.R., Real, C.R., and D.L. Parke, 1981, Preparation of isoseismal maps and summaries of reported effects for pre-1900 California earthquakes, *Calif. Div. Mines Geol. Open-File Report 81-11 SAC*, 182 p.

Tuttle, M.P., and L.R. Sykes, 1992, Re-evaluation of several large historic earthquakes in the vicinity of the Loma Prieta and peninsular segments of the San Andreas fault, California, Bull. Seismol. Am., 1802-1820.

Working Group on California Earthquake Probabilities, 1988, Probabilities of large earthquakes occurring in California on the San Andreas fault, U.S. Geological Survey Open-File Report, p. 62.

Working Group on California Earthquake Probabilities, 1990, Probabilities of large earthquakes in the San Francisco Bay Region, California: U.S. Geological Survey Circular, p. 51.

Working Group on California Earthquake Probabilities, 2003, Earthquake Probabilities in the San Francisco Bay Region: 2002–2031: U.S. Geological Survey Open-File Report 03-214.

Working Group on California Earthquake Probabilities, 2008, The Uniform California Earthquake Rupture Forecast, Version 2 (UCERF 2): U.S. Geological Survey Open-File Report 2007-1437, 95 p.

Working Group on Northern California Earthquake Potential, 1996, Database of potential sources for earthquakes larger than magnitude 6 in northern California: U.S. Geological Survey Open-File Report 96-705, p. 53 p. [http://quake.wr.usgs.gov:80/hazprep/NCEP/].

7.0 PUBLICATIONS AND CONFERENCE PROCEEDINGS

Streig, A.R., Dawson, T.E., and R.J. Weldon, II, *in press October 2013*, Paleoseismic evidence of the 1890 and 1838 earthquakes on the Santa Cruz Mountains Section of the San Andreas Fault, near Corralitos, CA, *Bulletin of the Seismological Society of America.*

Streig, A.R., Dawson, T.E., and R.J. Weldon II, 2012, Determining Earthquake Recurrence and Slip Over the Past 3 - 4 events on the Southern Santa Cruz Mountains Segment of the San Andreas Fault: Collaborative Research between Geological Sciences, University of Oregon and the California Geological Survey, Award G10AP00065 and G10AP00064, *U.S. Geological Survey Final Report*, http://earthquake.usgs.gov/research/external/research.php

Streig, A.R., Dawson, T.E., and R.J. Weldon II, 2012, Earthquake Recurrence and Deformation in the Last Four Events on the Santa Cruz Mountains Section of the San Andreas Fault., *Eos, Transactions American Geophysical Union, Fall Meeting, Abstract T21H-07, 2012*.

Dawson, T.E., Streig, A.R., and Weldon, R.J., 2012, Three Historical Earthquakes on the Southern Santa Cruz Mountains Section of the San Andreas fault: Insights from Three Paleoseismic Sites, *Seis. Res. Lett.*, Vol. 83, No. 2, 2012 SSA Ann. Meeting abs, p. 384.

Streig, A.R., Dawson, T.E., Fumal, T., and R.J. Weldon II, 2012, Determining Earthquake Recurrence and Slip Over the Past 3-4 events on the Southern Santa Cruz Mountains Segment of the San Andreas Fault; *USGS 9th Annual Northern California NEHRP Workshop, January 24-25, 2012*.